Radiation effects on the *D* to *G* Raman intensities of carbon nanotubes

Assel Aitkaliyeva,[1] Michael S. Martin,[2] Tres A. Harriman,[3] Daniel S. Hildebrand,[3] Don A. Lucca,[3] Jing Wang,[1] Di Chen,[2] and Lin Shao[1,2,*]

[1]*Department of Materials Science and Engineering, Texas A&M University, College Station, Texas 77843, USA*
[2]*Department of Nuclear Engineering, Texas A&M University, College Station, Texas 77843, USA*
[3]*School of Mechanical and Aerospace Engineering, Oklahoma State University, Stillwater, Oklahoma 74078, USA*

(Received 2 August 2012; revised manuscript received 8 April 2014; published 30 June 2014)

For carbon nanotubes irradiated with 140 keV He ions, the intensity ratio of the *D* to *G* Raman modes initially increases and then decreases with increasing ion fluence. A model is proposed to describe the competing effects between the reduction in crystal size, which increases the *D* band intensity with increasing fluence as a long-range order effect, and the reduction in the number of sixfold rings available for *D* mode vibration, which decreases the *D* band intensity with increasing fluence as a short-range order effect. The latter effect dominates when the length of the short-range order becomes comparable to the unit-cell dimensions as a result of ion bombardment. This suggests that the appearance of the maximum *D* to *G* intensity ratio coincides with the onset of structural amorphization. The model is supported experimentally by examination of irradiated nanotubes with transmission electron microscopy, and theoretically by Raman calculation based on density functional perturbation theory. A universal formula is proposed to describe D/G behaviors under arbitrary ion irradiation.

DOI: 10.1103/PhysRevB.89.235437 PACS number(s): 61.48.De, 61.72.Ff, 61.80.−x

I. INTRODUCTION

Ion beam modification is an important tool in manipulating the structure and properties of carbon nanotubes (CNTs) [1–7]. The large surface-to-volume ratios of nanomaterials, such as CNTs, affect their radiation response so that it is different from their bulk counterparts. Knowledge of the radiation response of carbon systems accumulated through previous modeling studies of graphite, such as displacement creation, defect formation, and crystalline-to-amorphous transition, requires experimental validation for use with CNTs. Classic methods used to quantify radiation response in bulk materials, such as channeling ion beam analysis, cannot be applied to nanomaterials; consequently, studies on CNTs have relied heavily on Raman spectroscopic analysis [8–15]. The Raman spectra of sp^2 hybridized carbon systems have several distinct modes, most notably the *D* mode (at $\sim$1340 cm^{-1}), *G* mode (at $\sim$1580 cm^{-1}), and the radial breathing mode (at 50–500 cm^{-1}) in CNTs [13–15]. The exact nature of these modes depends on material properties and environmental conditions [13].

It has been shown that the *D* mode is related to crystal defects, including pentagon-heptagon pairs, kinks, vacancies, impurities, and tube ends [8–15]. According to the Tuinstra-Koenig (TK) relation, the *D* mode intensity is inversely proportional to the crystal size of graphite [9]. In damaged graphite or CNTs, the crystal size can be understood as a mean free path, coherent length of phonons, or the average distance between neighboring defects [8,16]. In practice, structural defects are often quantitatively characterized using the intensity ratio of the *D* to *G* modes (hereafter referred to as the D/G ratio). The normalization of the *D* mode by the *G* mode intensity is based on the nature of the *G* mode, which does not involve defects [13–15]. Several studies on the effect of radiation on CNTs have shown that ion and γ irradiation can result in an increase of the *D* mode intensity [17–19]. Moreover, the intensity saturates at high fluences, a behavior explained by dynamic defect recombination [17,18]. These studies have assumed that the *D* mode intensity is linearly proportional to the number of defects, which is a commonly made assumption that has had no systematic validation. In an early study on neutron irradiated graphite, Tanabe *et al.* showed that D/G ratios deviate from a linear relationship [8]. This finding inevitably raises doubts for reports in which D/G ratios are assumed to be linear disorder indicators, especially at higher degrees of damage.

In the present study, a systematic investigation of the relationship between the Raman spectroscopic response and microstructural changes of CNTs over a wide range of damage levels was performed. Ion fluences were sufficiently high to cause an ordered-to-amorphous transition, which led to the appearance of a maximum in the D/G ratio and deviation from the TK relation. Instead of introducing a cutoff fluence, defining the range over which the TK relation is valid, a modified TK relation with a disorder function is proposed. The proposed model considers the reduction in number of sixfold rings as a radiation-induced short-range order effect, in addition to the long-range order effect that reduces crystal size. By fitting the Raman data with the proposed model, it was possible to extract the displacement creation efficiency per ion and the level of disorder corresponding to the maximum D/G intensity ratio.

II. EXPERIMENTAL PROCEDURE

Self-supporting CNT mats (NanoLab Inc., Waltham, MA) were used. The mats had a thickness of about 100 μm and were composed of multiwalled CNTs with nominal diameters of 30 nm and mean lengths of 10 μm. There was no specific step during the fabrication to separate metallic and semiconducting multi-walled nanotubes (MWNTs), therefore the mats have a mixture of both types. Electronic resistivity of the mats, on the other hand, was found to decrease upon heating, suggesting that semiconducting MWNTs are dominant. Ion irradiation

*lshao@tamu.edu

was carried out at room temperature in two sets of experiments. In one set, ion fluence was varied at a fixed ion flux, while in the other ion flux was varied at a fixed fluence. In the fluence dependence study, samples were irradiated with 140 keV He ions at a fixed flux of about 8×10^{12} cm^{-2} s^{-1} with fluences ranging from 1×10^{14} to 5×10^{16} cm^{-2}. In the flux dependence study, two fluences were selected, 5×10^{14} and 1×10^{16} cm^{-2}, and for each fluence, flux was varied from 3×10^{11} to 3×10^{13} cm^{-2} s^{-1}. Considering a mat density of 0.5 g/cm^3, the stopping and range of ions in matter (SRIM) code predicts a mean penetration depth of 2.8 μm for the 140 keV He ions [20]. Raman spectroscopy was performed using a Horiba Jobin-Yvon LabRam microscope with a 17 mW He-Ne laser at a wavelength of 632.8 nm, and a WITec confocal Raman microscope with a frequency doubled Nd:YAG laser at a wavelength of 532 nm. Excitation light was focused with a $10 \times$ /0.3 NA objective and the scattered light was recollected and focused onto a 100-μm-diam optical fiber acting as a confocal pinhole. Raman spectra were analyzed by fitting with Lorentzian and/or Breit-Wigner-Fano (BWF) functions using a least-squares algorithm. Transmission electron microscopy (TEM) was performed with a FEI TECNAI G^2 F20 ST FE-TEM operated at an accelerating voltage of 200 kV. The TEM specimens were prepared by sectioning with a microtome.

III. RESULTS AND DISCUSSION

Figure 1 compares the Raman spectra of samples before and after He ion irradiation to a fluence of 1×10^{16} cm^{-2}. As illustrated in the insets, the G mode arises from the in-plane bond stretching motion of pairs of C atoms, which does not require sixfold rings [9,15]. The G mode does not involve defects and its existence is expected regardless of whether sp^2 carbon materials are ordered or disordered [9,15]. The D mode arises from the breathing motion of sixfold rings and involves phonons near K zone boundaries, indicating the presence of disorder or boundaries [15]. Both the intensity and width of the D mode at 1337 cm^{-1} increased after irradiation, but no spectral shift was observed. In CNTs, the G mode can split into two distinct modes: a G^- mode associated with in-plane vibration in the direction of the CNT axis and a G^+ mode related to in-plane vibration along the circumferential direction [21]. The G mode of an unirradiated sample consisted of a G^- mode at 1597 cm^{-1} and a weaker G^+ mode at 1615 cm^{-1}, which was determined by fitting with Lorentzian functions. After ion irradiation, the G mode evolved into a wider, more asymmetric single peak, well described by a BWF fit (shown as a dotted line in Fig. 1) [22]. The BWF fit was originally introduced to describe the coupling between discrete Raman modes and a continuum background. The fit indicated the full width at half maximum (FWHM) was 53 cm^{-1} with a coupling factor of -0.28. The negative coupling factor suggests that the BWF fit should be used as an effective fitting method, rather than the proof of the physical meaning as it is indicated by the original model [22]. The peak center after irradiation was shifted by 10 cm^{-1} from the original G^- mode to 1587 cm^{-1}. This peak shift at low fluences was difficult to observe.

Figure 2 shows the normalized D/G ratio as a function of displacement-per-atom (dpa) values. The dpa values are converted from ion fluences. All D/G ratios were normalized by the D/G ratio of the unirradiated CNTs. Due to finite tube lengths and residual defects in pristine CNTs, a nonzero D mode intensity is expected. The normalized D/G ratio increased with ion fluence and reached a maximum at a fluence of 5×10^{15} cm^{-2}. Beyond this critical fluence, the D/G ratio decreased with further increase in fluence. The critical fluence of 5×10^{15} cm^{-2} corresponds to an average of 0.15 dpa in the damaged region, based on SRIM calculations and a displacement energy of 20 eV [23]. The appearance of a maximum D/G ratio suggests that using the D/G ratio to quantify the number of defects in CNTs becomes questionable at higher damage levels. This observation also suggests that the TK relation becomes invalid beyond a certain crystal size or requires modification.

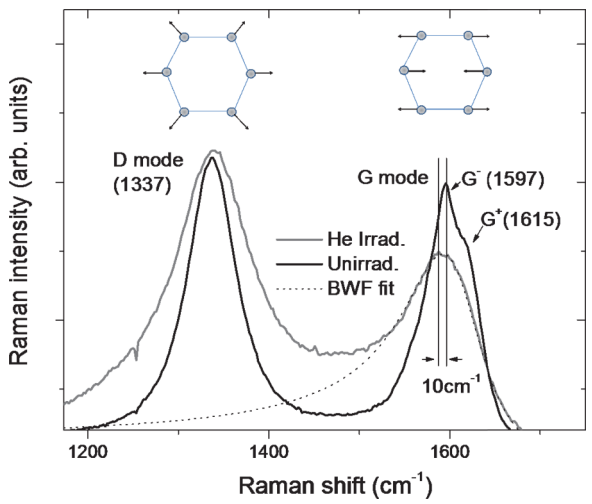

FIG. 1. (Color online) Raman spectra of CNTs before and after 140 keV He ion irradiation to a fluence of 1×10^{16} cm^{-2}. The dotted line denotes the BWF fit.

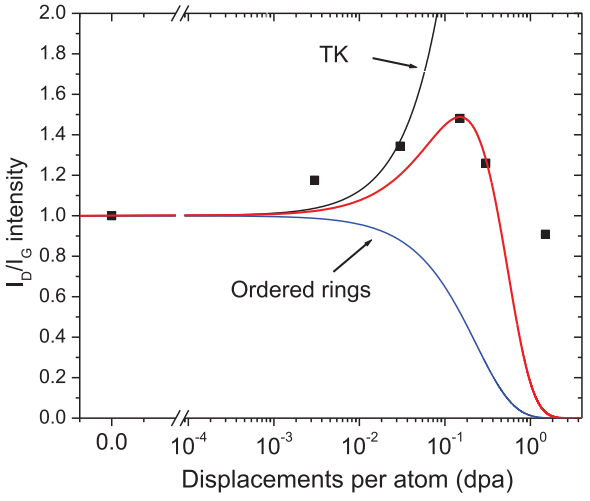

FIG. 2. (Color online) The normalized D/G ratios of He ion irradiated CNTs as a function of dpa values (equivalent to ion fluence). The solid lines represent data fit based on the model described in Eq. (2).

Near the critical fluence and beyond, crystal size effects predicted by the TK relation still play a role, but the D mode intensity is largely affected by the reduction in the number of ordered rings. Considering the statistical probability of repeatedly damaging disordered rings, an effect that can be ignored at low ion fluences but becomes important at high fluences, the rate change of ordered rings can be described by

$$dN/dn = -b(N_0 - N)/N_0, \tag{1}$$

where N is the number of ordered rings, N_0 is the total number of rings in an unirradiated sample, b is the efficiency of creating disordered rings by a single bombarding ion, and n is the ion fluence. This leads to the expression for the number of ordered rings as a function of ion fluence: $N(n) = N_0\exp(-bn)$. Based on a linear proportionality between the D intensity and N, a modified TK relation can be expressed as

$$I_{D/G}(n) = [C(\lambda)/L_a(n)][N(n)/N_0], \tag{2}$$

where $I_{D/G}(n)$ is the D/G intensity ratio as a function of ion fluence n, $C(\lambda)$ is the constant introduced in the TK relation, and L_a is the crystal size, which depends on n. The term $[C(\lambda)/L_a(n)]$ comes from the TK relation and the term $[N(n)/N_0]$ originates from the reduction of ordered rings. If the CNTs have not been irradiated ($n = 0$) and have no intrinsic defects, the CNT length represents the crystal dimension. The introduction of defects and damage cascades due to irradiation is equivalent to sectioning the CNT into segments. Thus the crystal size can be taken as the distance between defects and can be approximated as

$$L_a(n) = L/(an + n_0 + 1), \tag{3}$$

where L is the mean length of a CNT, and n_0 is the number of intrinsic defects in a CNT. The parameter a is introduced to describe the efficiency of damage creation per ion in a given CNT for a fluence n.

A fit of experimental data in Fig. 2 was performed using the proposed model by adjusting parameters a and b in Eqs. (2) and (3). Since the D/G ratios were normalized to that of the unirradiated CNTs, $C(\lambda)$ and L were not required for the fitting. Also shown with the fit in Fig. 2 are plots that take into account only the TK relation (black dashed line) and only ring destruction (red dashed line). There is a clear divergence of the TK relation and the proposed model at fluences above 1×10^{14} cm^{-2}. Reasonable agreement with experimental results was obtained at $a/(n_0 + 1) = 3.7\times10^{-16}$ cm^2 and $b = 1.3\times10^{-16}$ cm^2. Parameter b could be thought of as the cross section of sixfold ring destruction and should be comparable to the displacement creation cross section. The displacement creation cross section can be estimated using the box-based shape approximation. The displacement profile predicted by the SRIM code has a sharp Gaussian-like peak at a depth of 2.7 μm and a FWHM of about 0.5 μm, and there are about 135 displacements produced per ion. The average displacement creation cross section is calculated to be about 1.1×10^{-16} cm^2, which is comparable to the extracted b value from the data fitting. Furthermore, the maximum D/G ratio corresponds to $N(n)/N_0 = 0.5$, which is sufficiently high for an ordered-to-amorphous transition to occur.

Figures 3(a)–3(d) show transmission electron micrographs and filtered images after Fourier transformation for specimens

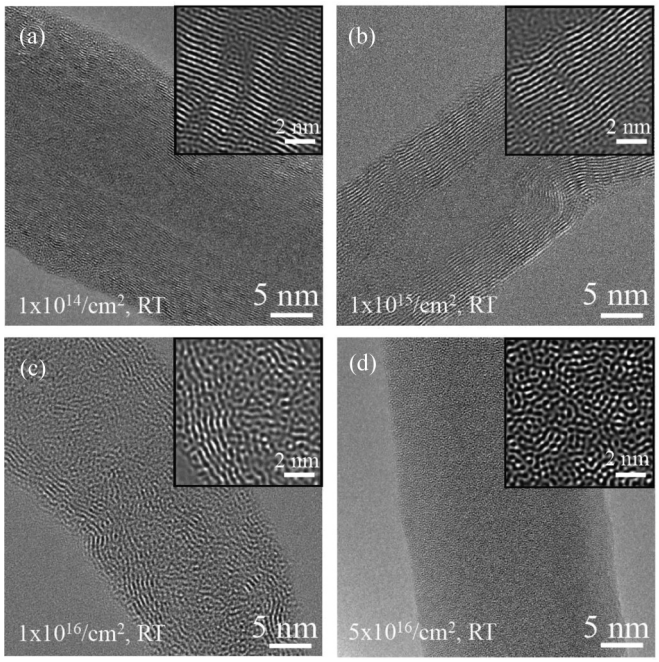

FIG. 3. TEM micrographs of CNTs irradiated with He ions to fluences of (a) 1×10^{14} cm^{-2}, (b) 1×10^{15} cm^{-2}, (c) 1×10^{16} cm^{-2}, and (d) 5×10^{16} cm^{-2}.

irradiated to fluences of 1×10^{14}, 1×10^{15}, 1×10^{16}, and 5×10^{16} cm^{-2}, respectively. As shown in Fig. 3(a), after irradiation to a fluence of 1×10^{14} cm^{-2}, well-ordered structure of the CNTs remains intact and no large damage zones are observed, but basal planes have been slightly disturbed. Figure 3(b) shows that at a fluence of 1×10^{15} cm^{-2}, trenchlike damage zones across CNT walls begin to develop as a result of increased basal plane disturbance. Figure 3(c) shows that at a fluence of 1×10^{16} cm^{-2} disordering is significant, and contains both mixing of basal planes and localized amorphization. At the highest fluence of 5×10^{16} cm^{-2} a collapsed structure is observed, as shown in Fig. 3(d). These observations confirm that significant damage/amorphization is initiated between 1×10^{15} and 1×10^{16} cm^{-2}.

Figure 4 shows the normalized D/G intensity ratio as a function of flux for the two fluences 5×10^{14} and 1×10^{16} cm^{-2}, which were chosen because they are on opposite sides of the critical fluence. The flux values are expressed as dpa per second. For the lower fluence the normalized D/G ratio decreased with increasing flux, while for the higher fluence the normalized D/G ratio increased with increasing flux. Since 5×10^{14} cm^{-2} (1.5×10^{-2} dpa) is below the critical fluence (0.15 dpa) and 1×10^{16} cm^{-2} (0.3 dpa) is above the critical fluence, the trends observed in Fig. 4 indicate that a higher flux leads to lower damage accumulation. This flux dependence can be explained by beam heating under high flux. Although the measured substrate temperature rise was less than 10 °C for the highest flux, dynamic defect annealing might be significant in localized regions due to damage cascade formation. Our previous work has suggested that defect annealing can be achieved in CNTs with an activation energy of about 0.36 eV [24]. However, the possibility of more complicated mechanisms cannot be ruled out. The flux

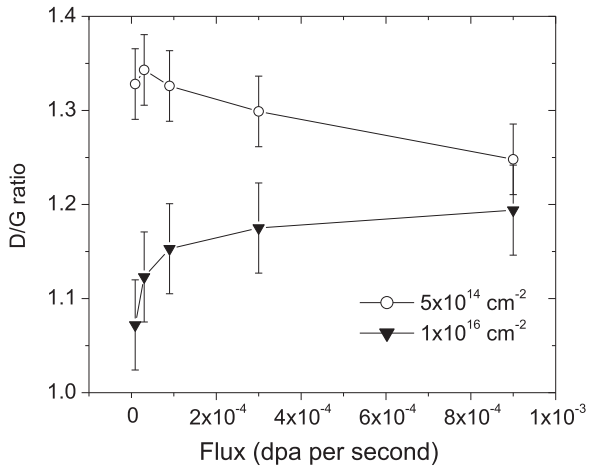

FIG. 4. The normalized D/G intensity ratios of He ion irradiated CNTs as a function of ion flux, at fixed fluences of 5×10^{14} and 1×10^{16} cm^{-2}. The error bars represent the statistical errors of the measurements. The ion flux values are converted to equivalent dpa per second.

dependence could be attributed to enhanced interstitial-vacancy recombination where interstitials from one ion track encounter vacancies created in another ion track before vacancies become sufficiently diluted. At low flux, vacancies spread away from the ion track, thus reducing defect recombination efficiency which is proportional to the product of interstitial and vacancy densities. This model was first proposed by Hallén *et al.* for damage created in Si with MeV proton irradiation, and could be applied here by considering that in both cases, light ions were used and similar damage patterns were created [25]. Both featured point defects, rather than large damage cascades.

The existence of a maximum D/G or D/G' intensity ratio in ion-irradiated CNTs and graphene have been previously observed [23,26–28], although a different phenomenological mode has been proposed by Lucchese *et al.* to explain the changes observed in the D/G ratio for ion-irradiated graphene [26]. Their model assumes that two types of defects contribute to the D mode intensity: Defects in "radiation-activated" A regions contribute most of the D mode intensity, while defects in "structurally disordered" S regions also contribute to the D mode intensity, but to a much lesser extent. The S regions correspond to the damage core of individual ion tracks, while the A region surrounds each core. Thus the D intensity is determined by the competing mechanism between areal coverage of two regions [26]. We need to point out that our model and conclusions presented in this study are substantially different than that from Lucchese *et al.* They abandoned the TK relation and concluded it was not valid for defect analysis in ion-irradiated graphene, while the present study reaches the opposite conclusion. Also, in order to achieve a maximum D/G ratio, the S region suggested by Lucchese *et al.* must contribute a weak, but nonzero D mode intensity. Without such a contribution the D/G intensity ratio will never decrease, but consequently their model predicts that the D mode intensity saturates to a nonzero value under extreme radiation. In a comparison, our model is based on the assumption that fully amorphized carbon should have zero D intensity, based on the simple fact that, if D mode vibration is associated with sixfold rings, the D mode must disappear if no sixfold rings exist [28].

Our model can be further extended to describe Raman behavior in graphene after a slight modification. Since graphene is a two-dimensional material, its crystal size, or average defect distance, should be described by

$$L = \sqrt{A/(an + n_0 + 1)}, \tag{4}$$

where A is the original graphene area, n is the ion fluence, n_0 is the number of intrinsic defects, and a is the cross section of atomic displacements per ion. To remove the complexity caused by the original dimensions and number of intrinsic defects, it is feasible to normalize $I_{D/G}(n)$ by the value obtained after irradiation at the lowest ion fluence, n_1. We therefore obtain

$$I^*_{D/G} = \frac{I_{D/G}(n)}{I_{D/G}(n_0)} = \begin{cases} \sqrt{c_1(n-n_1)+1} \times \exp[-c_2(n-n_1)] & \text{for graphene} \quad (5) \\ [c_1(n-n_1)+1] \times \exp[-c_2(n-n_1)] & \text{for CNT} \quad (6) \end{cases}$$

Figure 5(a) compares Raman data from Ref. [26] for Ar ion irradiated graphene and a fit of that data using Eq. (5). In Ref. [26] the Raman data was plotted as a function of crystal size L, instead of ion fluence. Therefore n and n_1 in Eq. (5) are replaced by $1/L^2$ and $1/L_1^2$, respectively, and data for $L_1 = 22.5$ nm was used for the normalization. The fitting parameters c_1 and c_2 are 4×10^{-11} cm^{-2} and 4×10^{-14} cm^{-2}, respectively. Overall, the fitting agrees well with the experimental data.

The proposed model can also be used to fit Raman data previously reported by others for CNTs. In order to provide a "universal formula" suitable for different ion irradiation conditions, Eq. (6) for CNTs can be changed to

$$I^*_{D/G} = [(c_1 \times \text{dpa}) + 1]\exp(-6\times\text{dpa}), \tag{7}$$

where dpa is the displacements per atom for the given irradiation conditions. The formula applies to the specific normalization condition that the D/G values are normalized by that of pristine CNTs [corresponding to $n_1 = 0$ in Eq. (5)]. The multiplication factor of 6 is introduced since a sixfold ring can be destroyed if any one of its six atoms is displaced. If we further assume that most of the D signals originate from the region having the highest damage, the dpa of the peak damaged region can be used. This value can be obtained by using the

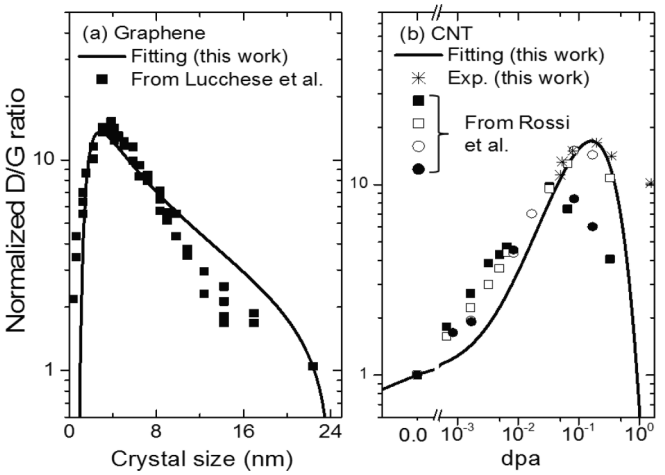

FIG. 5. (a) Normalized D/G intensity ratios from Ref. [26] for Ar ion irradiated graphene fit by the model given in Eq. (5), and (b) normalized D/G intensity ratios from Ref. [27] for P or B ion irradiated CNTs fit by the model given in Eq. (7). Experimental results from the present study are also plotted for comparison. For (a), the D/G values are normalized to the value corresponding to $L = 22.5$ nm. For (b), the D/G values are normalized to the value corresponding to the pristine CNTs.

SRIM code. The uniqueness of Eq. (7) comes from the fact that only one fitting parameter is needed for an arbitrary ion irradiation condition.

Figure 5(b) shows the Raman data for irradiated CNTs from Ref. [27] and a fit of that data using Eq. (7). The data includes four sets of experiments: 150 keV P ion irradiation of metallic CNTs (■), 150 keV P ion irradiation of semiconducting CNTs (□), 150 keV B ion irradiation of metallic CNTs (●), and 150 keV B ion irradiation of semiconducting CNTs (○). All Raman data was normalized to pristine CNT films. Using 20 eV as the displacement energy, the calculated peak dpa (normalized to one ion) for 150 keV P and 150 keV B are 6.6×10^{-16} and 1.7×10^{-16}, respectively. All four irradiations can be well fit using $c_1 = 270$. The parameter c_1 depends on the CNT properties, i.e., the number of defects in the pristine CNTs. Therefore, the c_1 value varies for different experiments. For example, our Raman data shown in Fig. 2 can be fitted well using Eq. (7) with $c_1 = 24$.

Figure 5(b) also includes the experimental data obtained from the present study. Our raw data, after being normalized by the $I_{D/G}$ of the unirradiated sample, is much less than the modeling prediction. We believe this is due to the fact that the unirradiated sample is not defect-free. In Fig. 5(b), we first multiply all our experimental $I_{D/G}$ data by a factor ($\sim$11) to match the modeling predicted peak $I_{D/G}$ value. Then all data is shifted by the same amount of dpa (0.05 dpa) for the best alignment with the modeling curve. In other words, our experimental data agrees with the modeling curve if we assume that our unirradiated sample contains 0.05 dpa damage. This is not a surprising assumption since TEM images of the pristine sample indeed show some defective zones prior to ion irradiation.

Although a reasonable agreement has been obtained between experimental data and our modeling prediction, fluctuations and deviations exist and such difference can come from various sources including the difference in starting materials, ion irradiation, and characterization parameters. Electronic excitation, which dominates the stopping mechanism of high energy light ions, may play a role but details are unclear. Furthermore, different ions have different defect tomographies which may lead to different Raman signals. Heavy ions create large damage cascades, whereas light ions create small damage cascades or separated point defects. For heavy-ion irradiation, destroyed sixfold rings are distributed in highly localized regions, instead of being widely scattered under light ion irradiation. Using dpa as the only variable in $I_{D/G}$ prediction may ignore these details.

To provide additional support to the experimental observations and hypothesis, nonresonant Raman activities were computed by combining density functional perturbation theory (DFPT) and the finite displacement method, as implemented in the CASTEP code [29,30]. DFPT computes the response of electrons to atomic structural changes when atoms are displaced along one direction. The intensity for each Raman-active mode is calculated by appropriate space averaging of the Raman cross section for the Stokes component of the ith mode for a given laser frequency [31]. The norm-conserving pseudopotential was used and the exchange-correlation functional was treated using a generalized gradient approximation [32]. The plane wave basis set cutoff was taken to be 500 eV and k-point separation was set to be 0.08 Å$^{(-1)}$. Periodic boundary conditions were applied to a unit cell having one (3,3) CNT containing 36 atoms.

Figures 6(a)–6(c) show the calculated Raman D and G modes of a virgin CNT, a CNT containing one single vacancy, and a heavily disordered CNT, respectively. Each

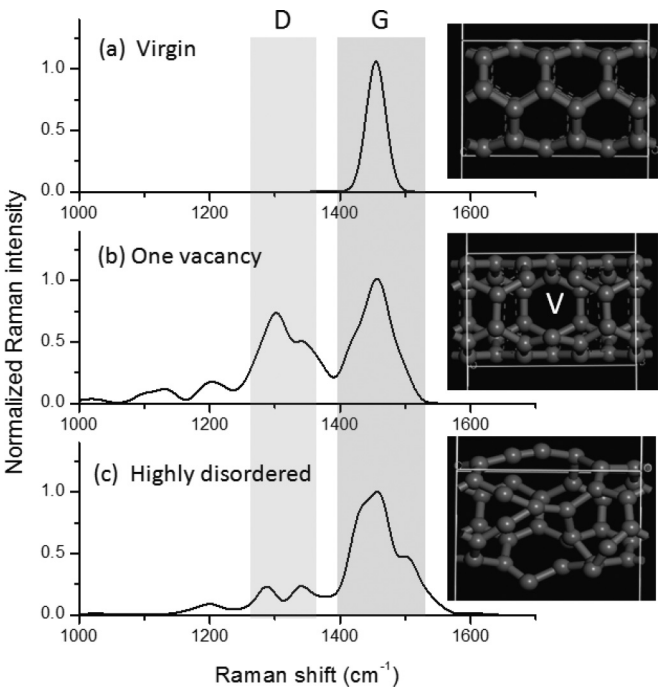

FIG. 6. Computed Raman spectra of (a) a pristine CNT, (b) a CNT with one vacancy, and (3) a highly disordered CNT. Insets show the CNT structure used as an input for the CASTEP code.

inset illustrates the input structures obtained from molecular dynamic (MD) simulations using the LAMMPS code [33]. All spectra are normalized using the G mode intensities. For the virgin CNT, only the G mode is present, which is in agreement with the theory that the D mode is related to boundaries and defects. As a result of size limits in the density functional theory (DFT) calculations, the calculated G mode peak is centered at $\sim$1450 cm^{-1}, which is about 150 cm^{-1} less than the experimental observation. Similar size dependence on G peak position has been reported before [34]. When the CNT contains one vacancy, multiple peaks appear with a strong peak at $\sim$1300 cm^{-1} corresponding to the D mode. Figure 6(c) simulates highly disordered CNTs with the majority of sixfold rings broken. The structure was obtained by heating a CNT up to 4000 K and then quenching to room temperature with subsequent structural relaxation by using the MD simulation code LAMMPS [33]. The AIREBO potential was used to describe C-C interactions [35] in the MD simulations. The relaxed CNT structure then was used as the input for the CASTEP code for Raman calculation. As shown in Fig. 6(c), the D mode intensity of the highly disordered CNT decreases compared to that of the CNT with a single vacancy. Although the modeling presented is limited to only three select conditions, the D/G intensity ratios were in agreement with the experimentally observed trends. We need to point out that the D mode intensity in Fig. 6(c) does not drop to absolute zero. This is due to the fact that not all sixfold rings are destroyed and highly distorted sixfold rings still exist in our amorphous structure obtained by annealing and quenching.

Rossi *et al.* further proposed to use the D/G' intensity ratio for the quantitative analysis of defect populations [27]. At relatively low defect levels, the G' mode intensity quickly decreases with increasing defect numbers, which improves its sensitivity for use in defect analysis. However, at high defect levels, particularly for irradiations with ion fluences close to or above where the maximum D/G ratio occurs, the G' mode is not easily observed. Therefore, no attempt was made here to discuss and fit variation in the D/G' ratio.

IV. SUMMARY

It has been shown that the TK relation can be extended to ultrafine crystal sizes without introducing a cutoff defining its validity region. In addition to the change in crystal size, the proposed model also considers the reduction in the number of ordered rings due to irradiation damage. The observed maximum in the D/G ratio occurred when the mean distance between defects or the crystal size used in the TK relation became comparable to the unit-cell dimensions, which correlated with the onset of an ordered-to-amorphous transition. Damage rate dependence of the D/G ratio has opposite trends for fluences below and above the critical fluence, and therefore care must be taken during Raman data interpretation. We further show that the model can be used to describe previously reported Raman data for graphene and CNTs. Based on our model, a universal formula with one fitting parameter was introduced to describe D/G changed in arbitrary ion irradiation conditions.

ACKNOWLEDGMENT

This work was supported by the U.S. Department of Energy, Office of Basic Energy Sciences, under Grant No. DE-SC0006725.

[1] A. V. Krasheninnikov and K. Nordlund, J. Appl. Phys. **107**, 071301 (2010).
[2] A. Kis, G. Csányi, J.-P. Salvetat, T.-N. Lee, E. Couteau, A. J. Kulik, W. Benoit, J. Brugger, and L. Forró, Nat. Mater. **3**, 153 (2004).
[3] J. A. Åström, A. V. Krasheninnikov, and K. Nordlund, Phys. Rev. Lett. **93**, 215503 (2004).
[4] F. Banhart, J. X. Li, and M. Terrones, Small **1**, 953 (2005).
[5] J. X. Li and F. Banhart, Nano Lett. **4**, 1143 (2004).
[6] B. Q. Wei, J. D. Arcy-Gall, P. M. Ajayan, and G. Ramanath, Appl. Phys. Lett. **83**, 3581 (2003).
[7] M. S. Raghuveer, A. Kumar, M. J. Frederick, G. P. Louie, P. G. Ganesan, and G. Ramanath, Adv. Mater. **18**, 547 (2006).
[8] T. Tanabe, Phys. Scr. **T64**, 7 (1996).
[9] F. Tuinstra and J. L. Koenig, J. Chem. Phys. **53**, 1126 (1970).
[10] B. S. Elman, M. Shayegan, M. S. Dresselhaus, H. Mazurek, and G. Dresselhaus, Phys. Rev. B **25**, 4142 (1982).
[11] G. Compagnini, G. A. Baratta, R. S. Cataliotti, and A. Morresi, J. Raman Spectrosc. **26**, 917 (1995).
[12] A. R. Adhikari, M. Huang, H. Bakhru, R. Vajtai, C. Y. Ryu, and P. M. Ajayan, J. Appl. Phys. **100**, 064315 (2006).
[13] A. Jorio, G. Dresselhaus, and M. S. Dresselhaus, *Carbon Nanotubes*, Topics in Applied Physics Vol. 111 (Springer-Verlag, Berlin, 2007).
[14] A. M. Rao, E. Richter, S. Bandow, B. Chase, P. C. Eklund, K. A. Williams, S. Fang, K. R. Subbaswamy, M. Menon, A. Thess, R. E. Smalley, G. Dresselhaus, and M. S. Dresselhaus, Science **275**, 187 (1997).
[15] A. C. Ferrari and J. Robertson, Phys. Rev. B **61**, 14095 (2000).
[16] K. Nakamura and M. Kitajima, Phys. Rev. B **45**,78 (1992).
[17] M. Hulman, V. Skákalová, S. Roth, and H. Kuzmany, J. Appl. Phys. **98**, 024311 (2005).
[18] V. Skákalová, J. Maultzsch, Z. Osváth, L. P. Biró, and S. Roth, Phys. Stat. Sol. (RRL) **1**, 138 (2007).
[19] M. Khanlary, R. Keshtmand, and M. Mojtahedzadeh, J. Theor. Appl. Phys. **4**, 40 (2010).
[20] J. F. Ziegler, J. P. Biersack, and M. D. Ziegler, *SRIM: The Stopping and Range of Ions in Matter* (Lulu Press, Morrisville, NC, 2009).
[21] M. S. Dresselhaus, G. Dresselhaus, R. Saito, and A. J. Jorio, Phys. Rep. **409**, 47 (2005).
[22] M. V. Klein, in *Light Scattering in Solids III*, edited by M. Cardona and G. Guntherodt, Topics in Applied Physics Vol. 51 (Springer-Verlag, Berlin, 1982).
[23] A. Aitkaliyeva and L. Shao, Carbon **50**, 4680 (2012).
[24] A. Aitkaliyeva, M. C. McCarthy, M. S. Martin, E. G. Fu, D. Wijesundera, X. Wang, W.-K. Chu, H.-K. Jeong, and L. Shao, Nucl. Instrum. Methods Phys. Res., Sect. B **267**, 3443 (2009).

[25] A. Hallén, D. Fenyö, B. U. R. Sundqvist, R. E. Johnson, and B. G. Svensson, J. Appl. Phys. **70**, 3025 (1991).
[26] M. M. Lucchese, F. Stavale, E. H. M. Ferreira, C. Vilani, M. V. O. Moutinho, R. B. Capaz, C. A. Achete, and A. Jorio, Carbon **48**, 1592 (2010).
[27] J. E. Rossi, C. D. Cress, A. R. Helenic, C. M. Schauerman, R. A. DiLeo, N. D. Cox, S. R. Messenger, B. D. Weaver, S. M. Hubbard, and B. J. Landi, J. Appl. Phys. **112**, 034314 (2012).
[28] A. C. Ferrari and J. Robertson, Philos. Trans. R. Soc., A **362**, 2477 (2004).
[29] V. Milmana, K. Refsonb, S. J. Clarkc, C. J. Pickardd, J. R. Yatese, S.-P. Gaof, P. J. Hasnipg, M. I. J. Probertg, A. Perlova, and M. D. Segall, J. Mol. Struct. **954**, 22 (2010).
[30] M. D. Segall, P. J. D. Lindan, M. J. Probert, C. J. Pickard, P. J. Hasnip, S. J. Clark, and M. C. Payne, J. Phys.: Condens. Matter **14**, 2717 (2002).
[31] D. Porezag and M. R. Pederson, Phys. Rev. B **54**, 7830 (1996).
[32] J. P. Perdew, K. Burke, and M. Ernzerhof, Phys. Rev. Lett. **77**, 3865 (1996).
[33] S. Plimpton, J. Comput. Phys. **117**, 1 (1995).
[34] J. Kürti, V. Zólyomi, M. Kertesz, G. Sun, R. H. Baughman, and H. Kuzmany, Carbon **42**, 971 (2004).
[35] D. W. Brenner, O. A. Shenderova, J. A. Harrison, S. J. Stuart, B. Ni, and S. B. Sinnott, J. Phys: Condens. Matter **14**, 783 (2002).